

## Internal current collection in microtubular SOFCs: Minimisation of contact resistance via brazing and plating

Item Type	Conference contribution
Authors	Hodjati-Pugh, Oujen;Dhir, Aman;Steinberger-Wilckens, Robert
Citation	Hodjati-Pugh, O., Dhir, A. and Steinberger-Wilckens, R. (2019) Internal current collection in microtubular SOFCs: Minimisation of contact resistance via brazing and plating, ECS Transactions, 91(1), pp. 533-548.
DOI	<a href="https://doi.org/10.1149/09101.0533ecst">10.1149/09101.0533ecst</a>
Publisher	The Electrochemical Society
Journal	ECS Transactions
Download date	2026-06-10 00:25:30
License	<a href="https://creativecommons.org/licenses/by-nc-nd/4.0/">https://creativecommons.org/licenses/by-nc-nd/4.0/</a>
Link to Item	<a href="http://hdl.handle.net/2436/622743">http://hdl.handle.net/2436/622743</a>

# **Internal Current Collection in Microtubular SOFCs: Minimisation of Contact Resistance via Brazing and Plating**

O. Hodjati-Pugh<sup>a</sup>, A. Dhir<sup>a,b</sup>, R. Steinberger-Wilckens<sup>a</sup>

<sup>a</sup>Centre for Fuel Cell and Hydrogen Research,

School of Chemical Engineering, University of Birmingham, B15 2TT

<sup>b</sup>School of Chemical Engineering, University of Wolverhampton, WV1 1LY

Microtubular Solid Oxide Fuel Cells ( $\mu$ -SOFC) are aptly suited for powering devices with demands ranging from the order of mW to few kW. The rapid start-up time, high thermo-mechanical stability, and excellent power density by volume lend them favour over alternate configurations, particularly for portable applications (1). Interconnecting the micro-tubes, though, is a persistent issue and minimisation of conduction pathway lengths and their contribution to stack ohmic resistance is a key parameter for maximising overall performance from a tubular cell stack (2). Contacting of each electrode is most simply and typically achieved from the cell exterior at the expense of available active electrode area. Exposing the cell support, interior electrode (anode or cathode, depending on cell configuration) from the exterior can lead to fuel crossover, decreasing fuel utilisation and giving rise to accelerated degradation from local thermal 'hot spots' as a result of hydrogen combustion (3).

In this paper a novel method of internal current collection is proposed to collect current from multiple points along the inner wall of an anode-supported tubular cell. The current collector will also act as a flow turbuliser, enhancing the flow and reducing thermal gradients within the fuel cell. Ensuring an intimate contact of the many current collection nodes to the anode and hence minimisation of contact resistance is achieved by use of brazing, depositing braze material via electroless plating. Interconnection proficiency has been studied using electrochemical performance testing, impedance spectroscopy, optical microscopy and mechanical testing.

## **Introduction**

To extract power from an SOFC cell, current collectors must be used at each electrode. The low voltage nature of fuel cells means that cells are typically stacked to achieve a useful power output by interconnecting current collectors of adjacent cells. An SOFC interconnect must have a low ohmic resistance, have a low contact resistance, high thermal conductivity, be inert in reducing/oxidising environments at high temperatures, have a similar coefficient of thermal expansion (CTE) to the different fuel cell components and be chemically compatible to the adjacent materials. The trend in

interconnect material selection, following the movement from high-temperature SOFC operation above 850°C to lower temperatures around 700 to 750°C has replaced the traditionally used ceramic perovskite-type materials such as  $\text{LaCrO}_3$  to Chromium-based steels or ferritic stainless steels (4).

Ceramic-based interconnects are brittle, costly and pose difficulty with respect to manufacture, shaping and cell assembly. Metallic interconnects, however, are less brittle, low cost and inherent ductility lends to facile shaping. Typical metallic interconnect materials include ferritic stainless steels such as Crofer 22A/APU/H and ITM, chromium-based materials such as CFY (5), austenitic steels such as 310 (6) and nickel-based alloys such as Haynes 230, favoured for its corrosion resistance over Inconel and Hastelloy counterparts (7–9). Metallic interconnects come with their own problems to overcome, namely the increase in area specific resistance (ASR) and decrease in mechanical properties resulting from reactivity in redox environments through high-temperature corrosion mechanisms (10–12). Studies to mitigate such degradation have focused around application of protective coatings and control of naturally formed oxide layer growth, particularly in stainless steels (13,14). A key advantage of metallic current collectors is the ability to be joined to the electrodes, with other current collectors (interconnection), and to stack components with standard welding or brazing techniques.

The high conductivity and mechanical durability of welded/brazed joints are ideal for use as a current collector-electrode joint, able to withstand long-term SOFC operation in portable and stationary applications, crucial for maximising fuel cell performance and durability. Some welded and brazed joints are gas-tight depending on the materials used, enabling use as a sealant, joining fuel cells to adjacent components such as manifolds, thereby offering higher ductility when compared to commonly used glass-ceramics, reducing the probability of failure due to thermally induced stress (13). Brazing is useful for areas where a welding flame cannot reach, such as the inner walls of a tubular fuel cell and avoids large spatial temperature gradients induced by localised ‘hot spots’ from the welding flame that can damage fuel cell components by inducing mechanical stress.

Brazing is used to bond two substrate materials, similar or not, by the addition of another filler material. The materials, specifically the joint, would be subject to heating (+450°C) from either a flame, electric heating elements or by induction to induce a phase change in the filler without impacting the substrate materials. Joining by brazing is possible if the liquid filler/braze will adhere to the solids to be joined. This adherence is known as wetting (15). The braze material must also be chosen to have similar CTE to the parent materials. Typical braze materials for use with SOFCs reported in literature are usually silver (16–18) for current collection (on both electrodes) or nickel-based on anodes (7,19) for both interconnection and sealing. Alloying materials include, but are not limited to, iron, copper, silicon, gold, titanium, palladium, platinum and chromium, and are added to adjust CTE, wettability, thermal/electrical conductivity, oxidation resistance. and strength (20). Silver-based brazes are higher in conductivity with respect to nickel-based materials, however, have high CTEs (w.r.t SOFC components) and studies have shown inadequacies of long-term stability of silver at high temperatures, also exhibiting gas permeability resulting in porosification, and internal formation of steam when exposed to redox environments (21,22). Nickel-based brazes are well suited for contacting SOFC anodes due to their material similarity, namely CTE and chemical

compatibility to commonly used Ni-YSZ cermets and their use are explored in this study (23).

## Scientific Approach

### Cell Specification

The micro-tubular SOFC cell used for the study was a state-of-the-art anode supported cell produced by Ultra Electronics (previously AMI). The Ni-YSZ anode was 152mm in length and had both a diffusion and reaction layer with total thickness of  $560\mu\text{m}$  thickness. A YSZ electrolyte,  $10\mu\text{m}$  in thickness, covered the entirety of the anode. Atop the electrolyte was an  $8\mu\text{m}$  thick GDC barrier layer, 101mm in length which supported a  $55\mu\text{m}$  thick LSCF cathode 95.5mm in length, giving an active cell area of approximately  $20\text{cm}^2$ .

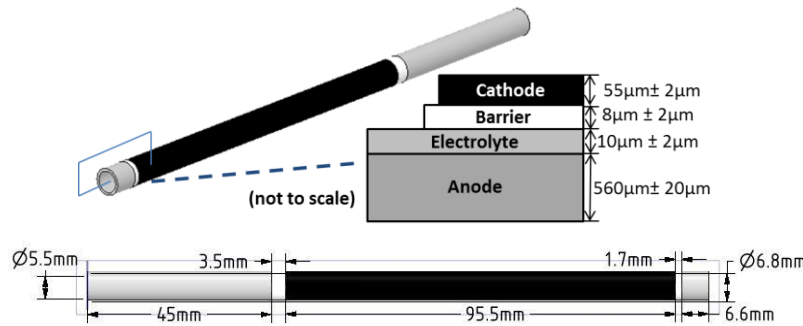


Figure 1.  $\mu$ -SOFC Geometry.

### Interconnect Specifications

Flow turbuliser technology designed by CalGavin, typically used in tubular heat exchangers has been used in this study for primary use as an internal current collector for  $\mu$ -SOFC. When used in heat exchangers, the hiTRAN turbuliser (hiTRAN) removes the laminar boundary layer by inducing turbulence in the tube side fluid, affecting the velocity and temperature distribution in order to reduce the resistance to heat transfer. This is particularly useful for low Reynold number flows which are well within the laminar region, typical in fuel cell applications where the flow rate is determined by the fuel utilisation of the electrochemical device. The hiTRAN turbuliser has a central core wire providing a backbone of support which is then threaded with a coil wire to create a repeating loop structure (24). Wire thickness, material, core length, coil length, outer diameter and loop section length and loop packing density (PD) can be varied to achieve an optimal design for the specific application.

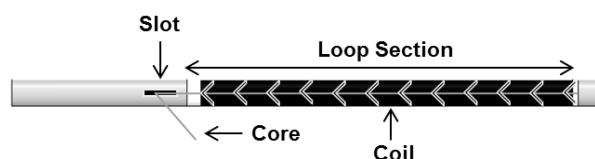


Figure 2. hiTRAN &  $\mu$ -SOFC Configuration.

In this study, the hiTRAN had a primary function as an interconnect, providing multiple contact points for current collection along the anode interior wall with a core wire that could be used as an interconnect, connecting to the cathode of an adjacent cell for stacking. The hiTRAN would also provide enhanced flow and thermal effects for the  $\mu$ -SOFC, increasing pressure drop along the cell and inducing turbulence which would directly affect mass transport within the anode. The turbulence would also affect the thermal gradients within the cell through enhanced convective heat transfer, combined with conduction effects from the metallic contact between the cell wall and the fluid within the anode flow channel.

Nickel was identified as an ideal material, particularly given the compatibility with the Ni-YSZ cermet anode material, low cost and inertness in the anode gas environment. The hiTRAN had to be designed considering its primary electrical function, and secondary function with respect to flow and thermal distribution. For the former, minimisation of ohmic resistance was the key optimising parameter, reducing bulk resistance and contact resistance. For the latter, maximising turbulence, pressure drop and heat transfer coefficient were key optimising parameters. Three different designs were trialled, varying only the packing density from a low packing density (LPD), to a medium packing density (MPD), and finally a high packing density (HPD). The total core length was 250mm, 115mm of which sat inside the cell acting as a support for the loop section with the remaining 'tail' used for interconnection to the cathode of an adjacent cell, exiting through a laser-cut slot in the inlet region of the cell. A packing section length of 100mm was selected to collect current from the entirety of the 95.5mm cathode length, determining the positioning of the hiTRAN within the cell. The outer diameter of the packing section was chosen to be oversized with respect to the 5.5mm tube bore, ensuring the hiTRAN was fixed firmly in position during assembly. To further secure the hiTRAN to the cell wall, brazing techniques were explored.

### Braze Specification

The choice of brazing material was based on (i) wettability to the parent materials, (ii) chemical compatibility to the parent materials, (iii) compatibility of brazing range to the operating temperature of the fuel cell, and (iv) compatibility with maximum allowable material temperature. Braze materials are selected and developed to ensure wetting can be achieved; they can be categorised as reactive and non-reactive, the former described by the Young equation (Equation 1). The contact angle  $\theta$  describes the relative contributions from two competing forces: (i) adhesion forces between solid-vapour ( $\sigma_{SV}$ ) and solid-liquid ( $\sigma_{SL}$ ) phases that promote wetting, and (ii) cohesion forces of the liquid ( $\sigma_{LV}$ ). The most common criteria to define whether brazing is applicable is whether a contact angle of less than  $90^\circ$  can be achieved (15).

$$\cos\theta = \frac{\sigma_{SV} - \sigma_{SL}}{\sigma_{LV}} \quad [1]$$

Given that the interconnect material was nickel and the anode cermet was nickel-based (Ni-YSZ), a nickel-based braze was chosen. Alloying materials such as boron, silicon, phosphorous, iron and chromium can be added to improve braze mobility/wetting, improve oxidation resistance, adjust hardness, adjust melting range and to act as melting point depressants, the latter crucial to avoid melting the nickel wires being brazed. Three

braze materials were identified as suitable by VBC Group LTD. The melting range of the braze materials is typically chosen to be 200°C higher than the joint will be exposed to in service.

Table I. Nickel-Based Braze Properties.

Product Name	Ni (wt%)	Cr (wt%)	Fe (wt%)	B (wt%)	Si (wt%)	P (wt%)	Melting Range (°C)	Suggested Brazing Temperature (°C)
AWS A58 (AMS)								
4770 (BNi-7)	Bal	14.0	-	-	-	10.1	960-1127	-
4776 (BNi-1a)	Bal	14.0	4.5	3.1	4.5	-	980-1070	1120
4777 (BNi-2)	Bal	7.0	3.0	3.1	4.5	-	970-1000	1060

The braze material BNi-2 was seen as the most promising option of the three in question. This was due to the favourably lower Cr content which is known to cause cathode poisoning (assuming volatilisation), the relatively small 30°C melting range that will suit the smaller-than-usual ramp rates required to protect the fuel cell components and the lower suggested brazing temperature. The BNi-2 braze material is suitable to both high temperature, high-stress components, heavy non-moving parts as well as honeycomb and thin materials, exhibiting very high joint strength and fluidity. The joint can withstand oxidation resistance up to 1060°C and has good corrosion resistance in a wide range of corrosive media (25).

A second brazing strategy incorporated electroless deposited nickel alloy solutions. A nickel-phosphorous alloy was chosen, whereby the phosphorous was selected to protect against corrosion and wear. Phosphorous levels were available in low (2-5wt%), medium (5-11wt%) and high (11-14wt%) quantity. Phosphorous also acts as melting point depressant, with an increasing phosphorous content decreasing the melting point from around 1200°C for low phosphorous alloys to 800°C for high phosphorous alloys. Increasing phosphorous content also increases material resistivity (26). Here a 20µm coating of medium phosphorous solution (6-9wt%) was chosen and was provided by Frost Electroplating.

Table II. Tested Braze Materials.

Product Name	Ni (wt%)	Cr (wt%)	Fe (wt%)	B (wt%)	Si (wt%)	P (wt%)	Brazing Range (°C)
4777 (BNi-2)	Bal	7.0	3.0	3.1	4.5	-	970-1000
Electroless Ni-P Braze	Bal	-	-	-	-	6.0-9.0	900-1100

## Experimental Approach

### Vacuum Brazing

Samples using BNi-2 braze were brazed under vacuum at Keptson LTD, using an R&D scale vacuum furnace provided by HTS Vacuum Furnaces. The hiTRAN loop section was sprayed with an acrylic binder and then dusted with BNi-2 braze material in its powder form, shaking off excess and drying at room temperature for 30 mins before loading into the fuel cell. The first sample, 'Sample 1' was given a low loading of 0.15 g of braze material while 'Sample 2' was given a higher loading of 0.20 g.

Samples were loaded into the vacuum furnace, secured with ceramic blocks and placed under a mesh shield. A three-stage evacuation process using first a mechanical, then roughing, and then diffusion pump brought the brazing chamber pressure to high vacuum conditions of  $5 \cdot 10^{-5}$  Pa before any heating to ensure the lowest possible oxygen content to avoid any oxidation. A ramp rate of  $10^{\circ}\text{C}/\text{min}$  was used for temperatures below  $800^{\circ}\text{C}$  as used in the testing procedure discussed later. For temperatures above  $800^{\circ}\text{C}$ , a  $2^{\circ}\text{C}/\text{min}$  ramp rate was used which is commonly applied for cathode sintering at temperatures up to  $1400^{\circ}\text{C}$ . The two-stage brazing profile can be seen in Figure 3, the first dwell was for 5min at  $450^{\circ}\text{C}$  to allow binder burn off, this was followed by a 5 min dwell at the brazing temperature of  $1060^{\circ}\text{C}$ .

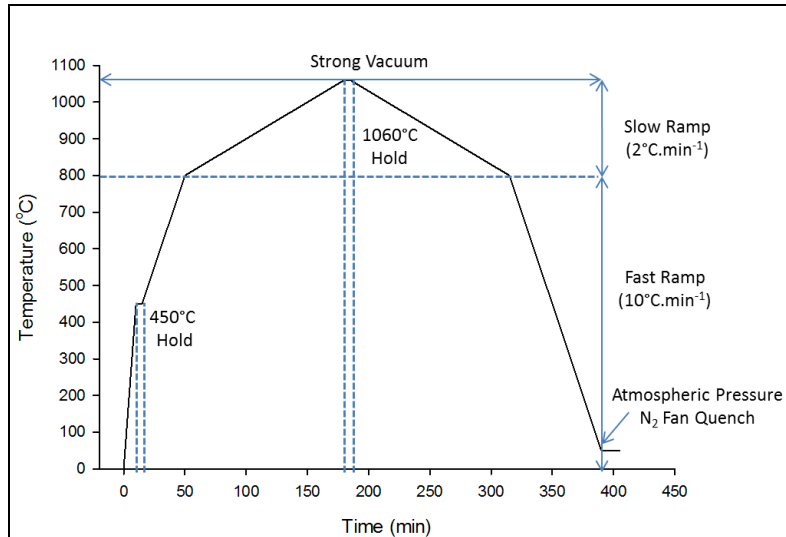


Figure 3. Vacuum Brazing Profile.

### Inert Brazing

Brazing using the electroless deposited Ni-P braze was done in an in-house rig seen in Figure 4, using a Vecstar horizontal tubular furnace. The pre-coated braze coated sample was loaded into the fuel cell and then loaded into a 1 m long, 20 mm outer diameter quartz brazing tube with vacuum stop valves at either end. The inlet stop valve was connected to an argon mass flow controller and argon cylinder, the outlet stop valve was attached to a bubbler to prevent reverse flow leading to the laboratory exhaust line. An argon flow rate of  $500 \text{ ml}\cdot\text{min}^{-1}$  was used, introducing the flow for 15 minutes before

following a similar profile to that in Figure 3, excluding the hold at 450°C and excluding strong vacuum conditions.

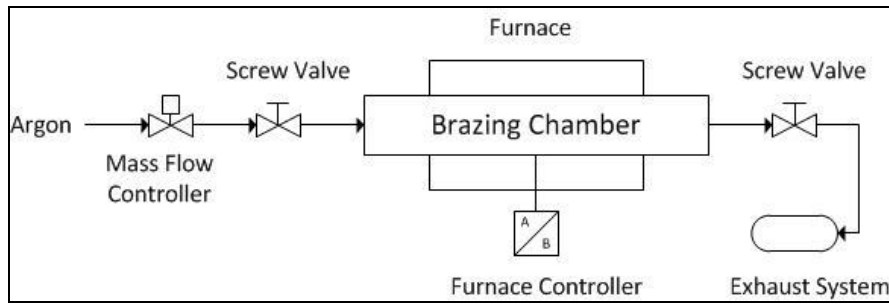


Figure 4. Inert Brazing Rig.

### Electrochemical Testing

The electrochemical performance was measured using a Solartron Analytical 1470E Cell Test System (Solartron) coupled to a Solartron Electrochemical Impedance Spectroscopy unit with a data logger using Cell Test software. The predicted current exceeded the maximum allowable current for a single input channel and so a Solartron 50V/25A booster system was used in series between the fuel cell and Solartron. An Elite Thermal Systems horizontal tubular furnace was used for non-brazing related cell preparation and fuel cell testing.

To extract current from the cell, electrode current collectors had to be attached in addition to gas manifolds. All cells tested, with or without the hiTRAN, had an external anode current collector for comparative purposes. The external anode connection was made by preparing an 8 mm wide connection point at the centre of the cathode length. The cathode and barrier layer were removed using a steel blade to shave layer by layer until the shiny, dense electrolyte was reached. A fine grain diamond tipped file was used to cut through the dense electrolyte to expose the dull grey anode. Braided silver/nickel wire was bound around the exposed anode and covered with a dense silver conductive paste applied with a fine artists brush. The paste was dried at room temperature for 30 minutes before furnace drying at 120°C for 1 hour. The cathode was covered in a porous silver paste, dried at room temperature for 30 minutes before furnace drying at 120°C for 1 hour. Braided silver wire was attached in a spine and band style, covered by a top layer of porous silver paste, and dried at room temperature for 30 minutes before furnace drying at 120°C for 1 hour. The setup is seen in Figure 5.

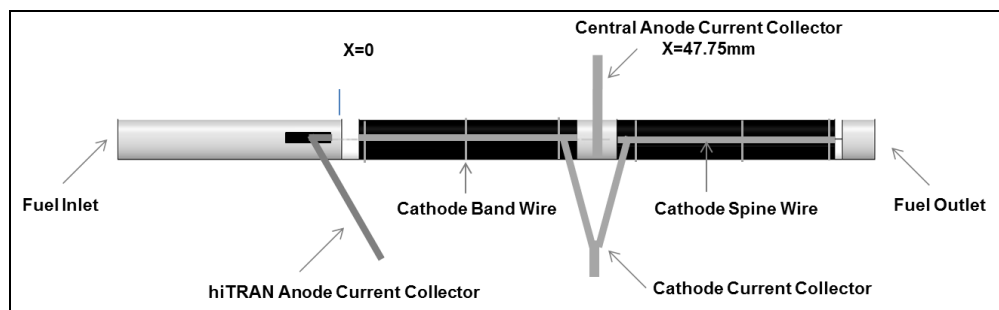


Figure 5. Electrochemical Testing Setup.

Alumina manifolds were used to supply fuel and remove exhaust gas and were secured to the cell using a ceramic adhesive. The fuel cell-manifold joints were cured at room temperature for 1 hour before heating to 93°C, dwelling for 2 hours and then to 260°C, dwelling for 2 hours before cooling to room temperature (10°C/min ramp throughout). Both the anode terminal and manifold joints were covered with a top coat of glass-ceramic sealing glass. The tail section of the hiTRAN exposed to the cathode environment was also coated with a top coat of sealing glass to prevent oxidation. The sealing glass was heated to 360°C with a 10°C/min ramp, dwelling for 1 hour before cooling to room temperature. Sintering of the sealing occurred during cell start-up. The cell was pressure tested for leaks before testing commenced.

Cells were tested with a furnace temperature of 750°C with 200 ml.min<sup>-1</sup> H<sub>2</sub> and 10 ml.min<sup>-1</sup> N<sub>2</sub>. At temperatures above 400°C a ‘safe gas’ mixture of 4% H<sub>2</sub> in N<sub>2</sub> was supplied to prevent anode oxidation. Air was provided to the cell by natural convection within the furnace chamber (Figure 6). Testing gas was introduced at 650°C, commencing the reduction/stabilisation step. Open circuit (OCV) measurement was commenced once the cell had reached the testing temperature, held for 1 hour to allow OCV stabilisation before any current was drawn with an OCV reading above 1 V, a requirement for any testing to proceed. The response of current with a change in potential was measured using a potential stair-step function. Constant potential measurements were taken at OCV, 0.9V, 0.7V and 0.5V. Impedance was measured to give insight on the contribution of current collection to the ohmic resistance of the fuel cell and was measured at OCV, 0.9V, 0.7V and 0.5V, with a frequency range between 1Hz and 10<sup>6</sup> Hz. Current collector conductivity was measured offline using a TTI BS407 Precision Milli/Micro Ohmmeter.

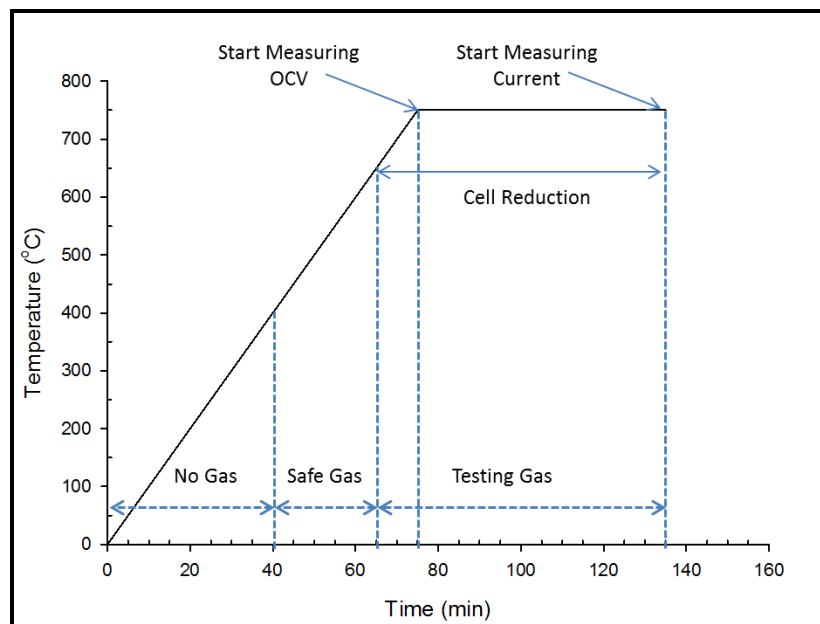


Figure 6. Start-up and Testing Profile.

## Mechanical Testing

To determine the strength of the joints between the hiTRAN and the cell wall an Instron 5848 Environmental Mechanical Tester (Instron) was used for tensile tests. The Instron had a fixed vice grip at its base with an upper vice grip attached to a load cell. The load cell could be changed depending on the force required; here a 100 N load cell was used.

The brazed hiTRAN and insert were loaded into an in-house fabricated metal cell holder which could then be sat in the base vice grip of the Instron without crushing the cell. The tubular cell holder had an 8 mm outer diameter with a stop at the end which only the wire could pass through to be held in the vice grip of the upper load cell. Bluehill software was used to control the Instron, setting the extension rate at 2 mm per minute with a maximum extension of 20 mm.

## Characterisation

To characterise the effect of brazing on the parent materials, and to inspect the braze material itself, optical microscopy was used. The optical microscope was a Zeiss AX10 Lab A1 and allowed up to 20x magnification; it was combined with Image-Pro Insight software for 3D analysis, ideal for looking for witness of joints.

## **Results and Discussion**

The mass and ohmic resistance of the hiTRAN increase as the packing density increases, as seen in Figure 7. This increase is due to more material being present in a unit length which is not favourable in terms of reducing cost, mass, ohmic resistance, and ultimately power density by mass. However, increasing the packing density will increase the number of contact points for current collection, meaning shorter pathway for electrons, flowing shorter distance through the less conductive anode, instead of flowing through the nickel hiTRAN to be extracted. The 20  $\mu\text{m}$  coating of Ni-P braze material weighed approximately 0.18 g giving a 10% increase in current collector mass

The ohmic contribution to the overall cell resistance was measured by recording the high-frequency x-axis intercept of the Nyquist plot obtained from impedance spectroscopy. Given that the fuel cells tested were from the same batch and were set up for testing in the same way, it was assumed that the contribution to the overall ohmic resistance from the electrolyte would be constant, and so any shift in value would be as a result of a change in the ohmic contribution from current collection. Figure 8 gives the high-frequency intercept value for un-brazed hiTRAN with LPD, MPD and HPD recorded at a cell potential of 0.9V. The impedance measured at 0.9V came from the region in the iV-curve dominated by ohmic resistance.

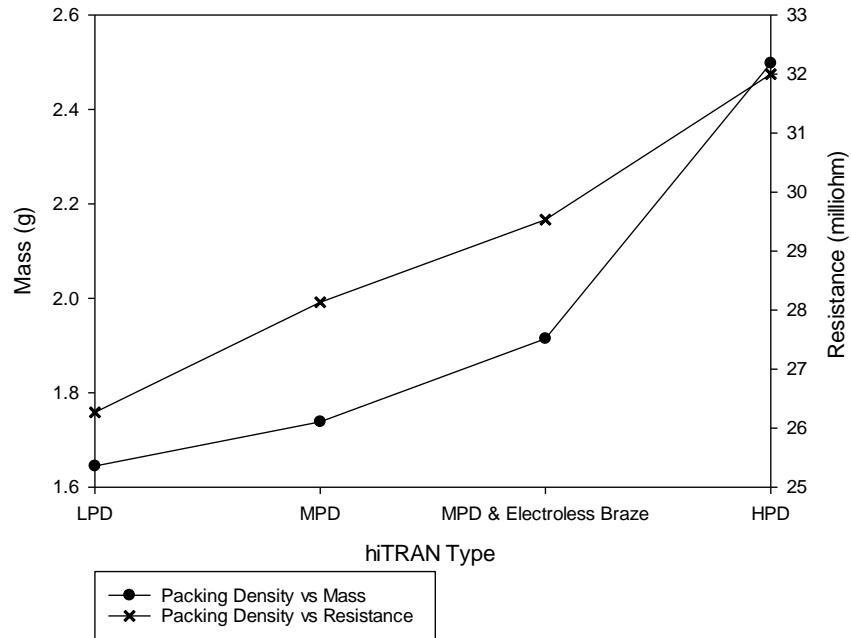


Figure 7. hiTRAN Packing Density vs Mass and Resistance.

The impedance values of the MPD and HPD were comparable and both measured  $0.23 \Omega$  to two significant figures. The lowest loop density gave the highest impedance of  $0.27 \Omega$  and yet had the lowest ohmic resistance recorded in Figure 7, highlighting the importance of increasing the number of contact points to reduce current collector resistance. Given the similar ohmic resistance between MPD and HPD, the MPD was chosen for brazing and electrochemical testing for its favourably lower mass (-40%) and cost of materials.

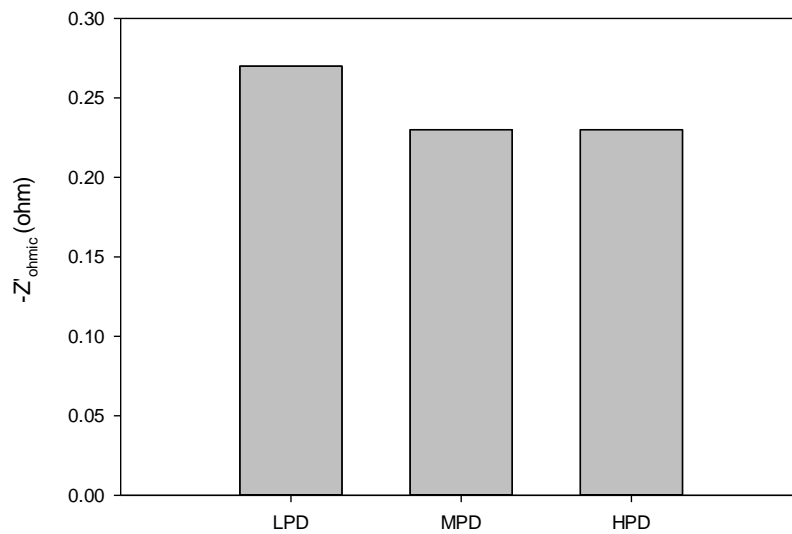


Figure 8. Cell Ohmic Resistance vs. hiTRAN Packing Density (Low, Medium, High).

IV measurement was conducted on the SOFC micro-tube, varying the current collector leads between the hiTRAN, a central (exterior) current collector made from nickel, and then a combination (in parallel) of the hiTRAN and central nickel current collector. Measurements at each current collector position were taken as close as possible to each other (with respect to time) to avoid any influence of cell performance degradation between measurements. Collecting current from the hiTRAN only gave the lowest performance with a power density at 0.7 V of 0.0573 W.cm<sup>-2</sup> and a maximum power density of 0.061 W.cm<sup>-2</sup>. A higher power density of 0.0734 W.cm<sup>-2</sup> at 0.7 V was observed at the central current collector with the maximum power density being 0.0783 W.cm<sup>-2</sup>. The highest power density came from the combination of the hiTRAN and central current collector with the power density at 0.7 V being 0.102 W.cm<sup>-2</sup> and a maximum power density of 0.1088 W.cm<sup>-2</sup>. Using a combination of hiTRAN and central nickel connector gave 39% higher maximum power output when compared to a central nickel connection and 78% higher maximum power output when compared to just a hiTRAN. The area specific resistance (ASR) was calculated for each iV-curve by calculating the gradient (assuming it to be approximately linear) in the region between 0.9 V and 0.6 V which was assumed to be dominated by ohmic losses. The ASR for hiTRAN only was calculated to be 22.2 Ω.cm<sup>2</sup>, the ASR for the central current collector is 15.2 Ω.cm<sup>2</sup>, and the ASR for hiTRAN and central current collection was 13.77 Ω.cm<sup>2</sup>.

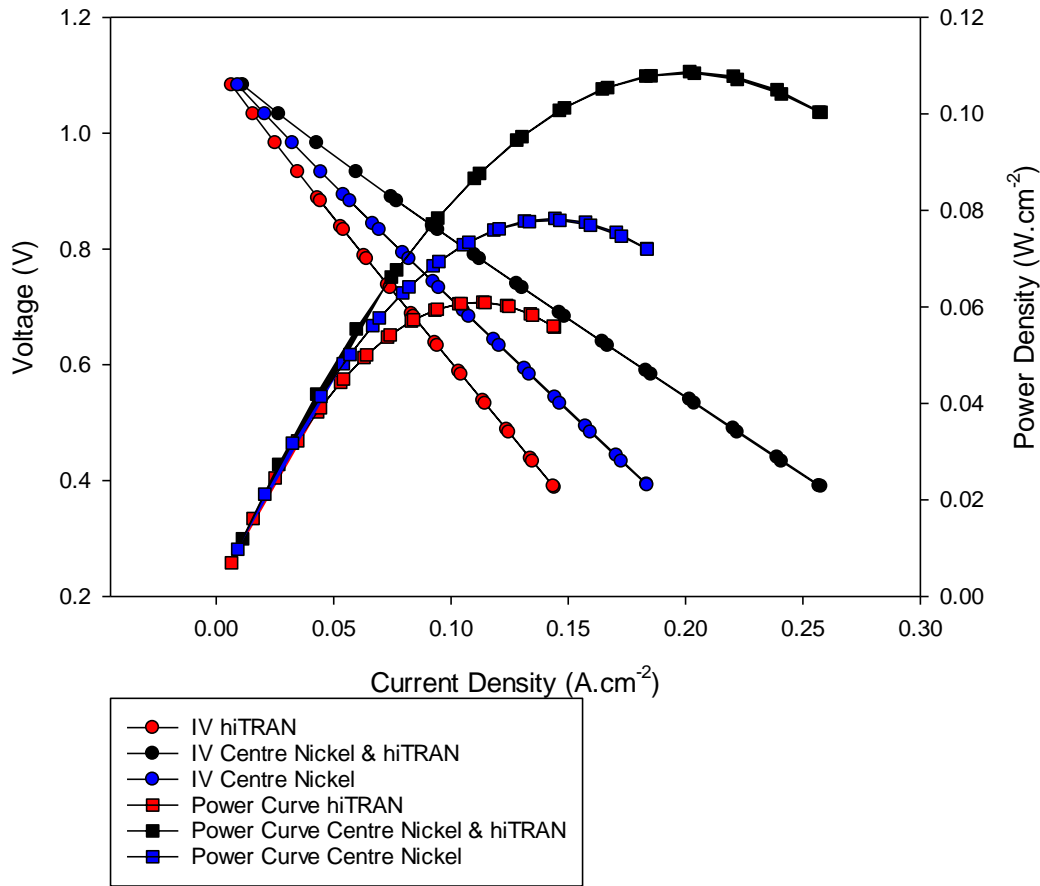


Figure 9. IV and Power Curve - hiTRAN MPD, Central Nickel and the two combined.

The contribution to the overall ohmic resistance of brazed versus un-brazed cells can be observed in Figure 10. The results are from inert brazed cells using the electroless deposited nickel-phosphorus solution. The impedance measurements presented were taken at OCV before any current had been drawn to ensure that the electrode-hiTRAN joint was in the best possible condition and had not been subject to local heating while conducting current. The bulk resistance of the hiTRAN was increased by 5% to 29.5 mΩ upon addition of the Ni-P, however, from impedance spectroscopy it was determined that the un-brazed hiTRAN gave an ohmic resistance of 0.21 Ω, which was reduced 126% to 0.093 Ω when brazed in an inert environment which can be attributed to a reduction in contact resistance between the electrode and hiTRAN.

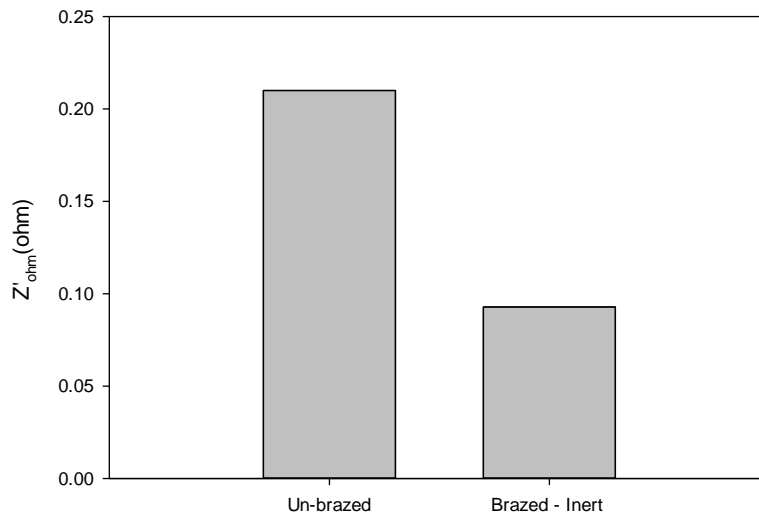


Figure 10. Ohmic Resistance of  $\mu$ -SOFC with hiTRAN un-brazed vs. brazed.

IV measurement was conducted on fuel cells that had hiTRAN un-brazed and inert brazed using the electroless nickel-phosphorous solution. The power density at 0.7 V increased by 117% from 0.0565 W.cm<sup>-2</sup> for the un-brazed sample to 0.1224 W.cm<sup>-2</sup> for the brazed sample while the maximum power density increased by 134% from 0.0611 W.cm<sup>-2</sup> to 0.1430 W.cm<sup>-2</sup> for the un-brazed and brazed samples, respectively. The ASR estimated by the gradient method between 0.9 V and 0.6 V was 19.95 Ω.cm<sup>2</sup> for the un-brazed sample, decreasing to 18.35 Ω.cm<sup>2</sup> for the brazed sample.

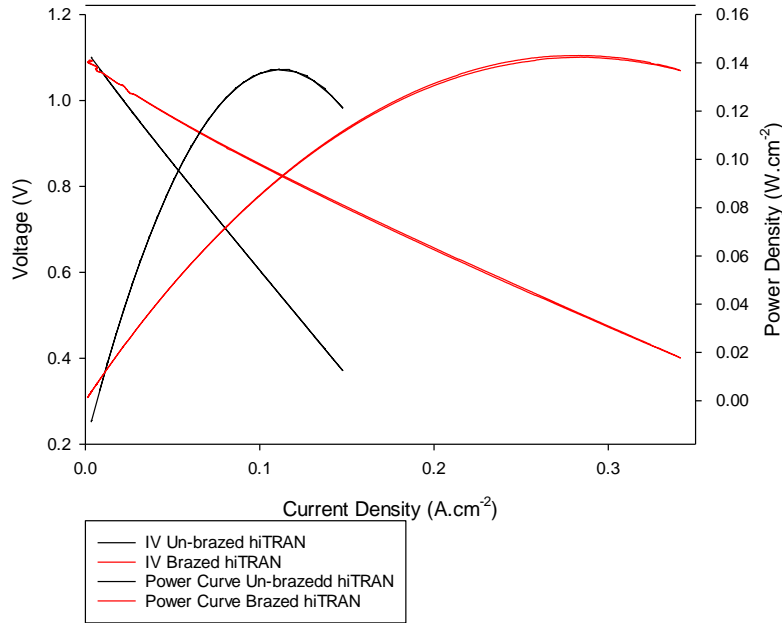


Figure 11. IV and power density curves - hiTRAN Medium un-brazed vs. brazed.

The images in Figure 12 show the witness of the joint between the hiTRAN and the interior anode wall. The depression occurred when the hiTRAN was removed from the  $\mu$ -SOFC, removing a section of material to which it was joined. Witness of this type was observed at multiple points along the cell wall of the fuel cell, indicating a mechanically strong electrode-hiTRAN joint.

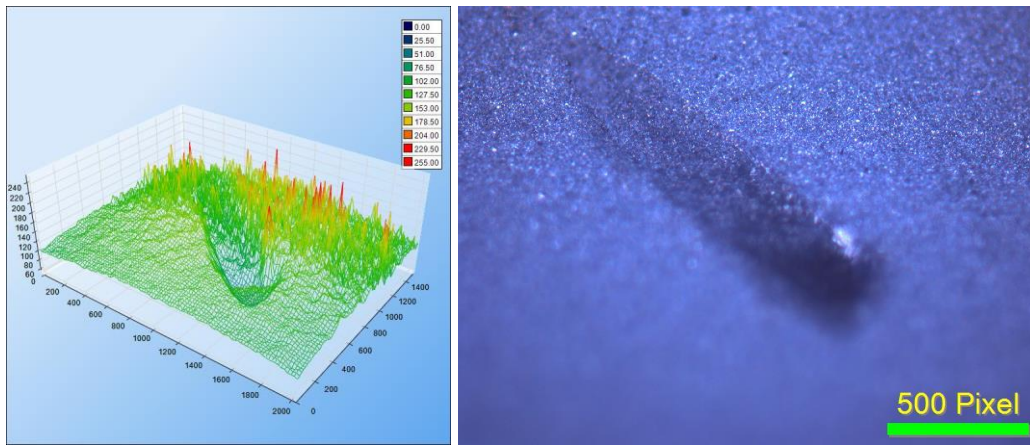


Figure 12. Optical Microscope Image & 3D render of Vacuum Brazed (4777) Joint Witness

Mechanical testing was only conducted on samples of vacuum brazed cells to date. The failure force required to completely separate the hiTRAN from the cell wall was measured to be 45 N for 'Sample 1', increasing by 33% to 68 N for 'Sample 2' which had a 33% higher loading of the brazing material. These values were sufficiently high to withstand the typical forces occurring in SOFC operation in both stationary and portable application.

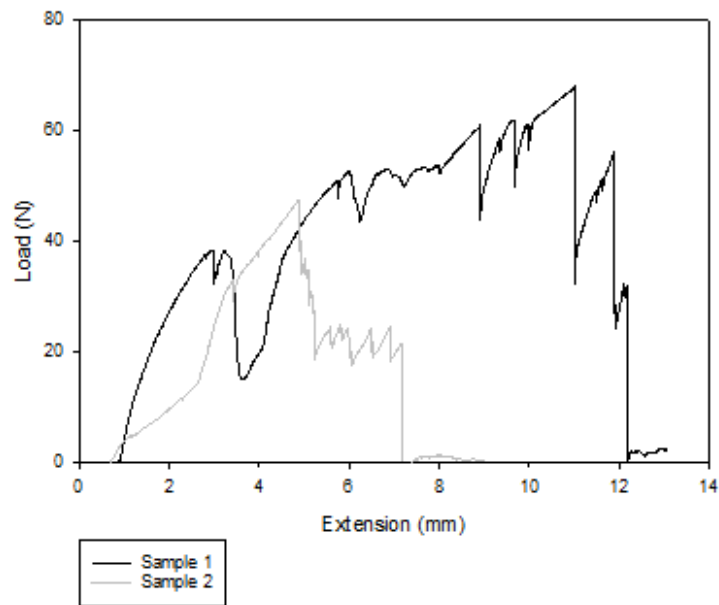


Figure 13. Load vs Extension Curve of Vacuum Brazed Samples (4777)

### Concluding Remarks and Further Work

Novel internal current collection of a  $\mu$ -SOFC was achieved, improving the maximum power output by 34% from a sole external current collection point. The minimisation of ohmic resistance of the internal current collector-electrode joint was achieved by an inert brazing technique, reducing the overall cell ohmic resistance by 126% through minimisation of the contact resistance between the current collector-electrode interfaces. This brazing technique led to a maximum power increase of 134% over an un-brazed counterpart. Joint witness was observed at multiple points along the cell interior and the internal current collector was fixed firmly in place throughout the service of the fuel cell. Mechanical testing was conducted on vacuum brazed samples, quantifying the joint strength between the multiple contact nodes of the current collector to the interior anode wall/support. Further work to quantify the strength of the electroless deposited Ni-P braze must be conducted as a comparison. The maximum power density of the fuel cell with hiTRAN current collection must be significantly improved to give a useful power output comparable with those reported in the literature. It should be noted that silver, a commonly used  $\mu$ -SOFC current collector material, with an order higher conductivity than nickel was not used in this study in an attempt to reduce cell level current collector cost, multiplied on a stack scale, to improve commercial. To improve the performance of hiTRAN as a current collector technique to reduce the bulk resistance will be explored, keeping the cheap, thermo-mechanically favourable nickel as a base material, plating with thin layers of highly conductive metals such as gold and silver.

## Acknowledgement

This work was supported by the Centre for Doctoral Training (CDT) in Fuel Cells and their Fuels, part-funded by the EPSRC. Acknowledgements go to CalGavin LTD for the supply of hiTRAN, the VBC Group LTD for braze material supply and brazing advice, and to Frost Electroplating LTD for supply of electroless nickel coating.

## References

1. Kendall K, Kendall M, Kendall K. 10 – Portable early market SOFCs. In: High-Temperature Solid Oxide Fuel Cells for the 21st Century. 2016. p. 329–56.
2. Aydin Ö, Koshiyama T, Nakajima H, Kitahara T. In-situ diagnosis and assessment of longitudinal current variation by electrode-segmentation method in anode-supported microtubular solid oxide fuel cells. *J Power Sources*. 2015;279:218–23.
3. Howe KS, Hanifi AR, Kendall K, Zazulak M, Etsell TH, Sarkar P. Performance of microtubular SOFCs with infiltrated electrodes under thermal cycling. *Int J Hydrogen Energy* [Internet]. 2013;38(2):1058–67. Available from: <http://dx.doi.org/10.1016/j.ijhydene.2012.10.098>
4. Kendall K, Kendall M, Niewolak L, Tietz F, Quadackers WJ. 7 – Interconnects. In: High-Temperature Solid Oxide Fuel Cells for the 21st Century. 2016. p. 195–254.
5. Transactions ECS, Society TE. Long Term Performance of Stacks with Chromium-based Interconnects (CFY) M. Brandner. 2013;57(1):2235–44.
6. Niewolak L, Wessel E, Singheiser L, Quadackers WJ. Potential suitability of ferritic and austenitic steels as interconnect materials for solid oxide fuel cells operating at 600 °C. *J Power Sources* [Internet]. 2010;195(22):7600–8. Available from: <http://dx.doi.org/10.1016/j.jpowsour.2010.06.007>
7. Casteel M. HYBRID MATERIALS DESIGN By. 2012;2012(August).
8. Hammer JE, Laney SJ, Jackson RW, Coyne K, Pettit FS. The Oxidation of Ferritic Stainless Steels in Simulated Solid-Oxide Fuel-Cell Atmospheres. 2007;67(February):1–38.
9. Jablonski PD, Alman DE. Oxidation resistance and mechanical properties of experimental low coefficient of thermal expansion (CTE) Ni-base alloys. 2007;32:3705–12.
10. Linder M, Hocker T, Holzer L, Friedrich KA, Iwanschitz B, Mai A, et al. Model-based prediction of the ohmic resistance of metallic interconnects from oxide scale growth based on scanning electron microscopy. *J Power Sources* [Internet]. 2014;272:595–605. Available from: <http://dx.doi.org/10.1016/j.jpowsour.2014.08.098>
11. Blennow P, Hjelm J, Klemensø T, Ramousse S, Kromp A, Leonide A, et al. Manufacturing and characterization of metal-supported solid oxide fuel cells. *J Power Sources* [Internet]. 2011;196(17):7117–25. Available from: <http://dx.doi.org/10.1016/j.jpowsour.2010.08.088>
12. Zhao F, Virkar A V. Dependence of polarization in anode-supported solid oxide fuel cells on various cell parameters. *J Power Sources*. 2005;141(1):79–95.
13. Bianco M, Linder M, Larring Y, Greco F, Van J. Lifetime Issues for Solid Oxide Fuel Cell Interconnects [Internet]. *Solid Oxide Fuel Cell Lifetime and Reliability*. Elsevier Ltd; 2017. 121-144 p. Available from: <http://dx.doi.org/10.1016/B978-0->

08-101102-7.00007-6

14. Froitzheim J, Canovic S, Nikumaa M, Sachitanand R, Johansson LG, Svensson JE. Long term study of Cr evaporation and high temperature corrosion behaviour of Co coated ferritic steel for solid oxide fuel cell interconnects Author's personal copy. 2012;220:217–27.
15. Dusan. P. Sekulic. *Advances in Brazing: Science, Technology and Applications*. 2013.
16. Sammes NM, Du Y, Bove R. Design and fabrication of a 100 W anode supported micro-tubular SOFC stack. *J Power Sources*. 2005;145(2):428–34.
17. Khan TI. Reactive brazing of ceria to an ODS ferritic stainless steel. 2003;8:2483–8.
18. W. Kobsiriphat SB. Ag-Cu-Ti Braze Materials for Sealing SOFCs. *J Fuel Cell Sci Technol*. 2008;5(1).
19. Lee S-B, Lim T-H, Song R-H, Shin D-R, Dong S-K. Development of a 700 W anode-supported micro-tubular SOFC stack for APU applications. 2008;
20. Tucker MC, Jacobson CP, Jonghe LC De, Visco SJ. A braze system for sealing metal-supported solid oxide fuel cells. 2006;160(February):1049–57.
21. Singh P, Yang Z, Viswanathan V, Stevenson JW. Observations on the Structural Degradation of Silver During Simultaneous Exposure to Oxidizing and Reducing Environments. *J Mater Eng Perform*. 2004;13(3):287–94.
22. Majewski AJ, Dhir A. Application of silver in microtubular solid oxide fuel cells. *Mater Renew Sustain Energy* [Internet]. 2018;1–13. Available from: <https://doi.org/10.1007/s40243-018-0123-y>
23. Kendall K, Kendall M, Cassidy M, Connor PA, Irvine JTS, Savaniu CD. 5 – Anodes. In: *High-Temperature Solid Oxide Fuel Cells for the 21st Century*. 2016. p. 133–60.
24. Murray J. Pressure loss and heat transfer for single-phase turbulent flow in tubes fitted with wire-matrix inserts. 2009.
25. Paper T, Weinstein M, Manager TS, Lee L, Johnson L, Engineer TS, et al. Properties of Selected Nickel and Iron Based Brazing Filler Metals. 2015;(April).
26. Cui G, Li N, Li D, Zheng J, Wu Q. The physical and electrochemical properties of electroless deposited nickel – phosphorus black coatings. 2006;200:6808–14.